Received 29 August 2020; revised 29 September 2020; accepted 29 September 2020.
Date of publication 12 October 2020; date of current version 29 October 2020.

Digital Object Identifier 10.1109/OJCOMS.2020.3030118

Implementation of Linearly Pulse Shaped Generalised Frequency Division Multiplexing for Visible Light Communication Systems

VEJANDLA KISHORE [1] (Member, IEEE), VENKATA MANI VAKAMULLA [1] (Senior Member, IEEE), WASIU O. POPOOLA [2] (Senior Member, IEEE), AND ABHINAV KUMAR [3] (Senior Member, IEEE)

[1]Department of Electronics and Communication Engineering, National Institute of Technology, Warangal 506004, India

[2]School of Engineering, Institute for Digital Communications, University of Edinburgh, Edinburgh EH8 9YL, U.K.

[3]Department of Electrical Engineering, Indian Institute of Technology Hyderabad, Hyderabad 502285, India

CORRESPONDING AUTHOR: V. KISHORE (e-mail: kishorevejandla@student.nitw.ac.in)

This work was supported in part by Science and Engineering Research Board (SERB), New Delhi, under Grant EMR/2016/7687, in part by the Ministry of Human Resource Development–Government of India under Grant SPARC (2019/249) and Grant SERB IMRC/AISTDF/CRD/2019/000178, and in part by the Department of Science and Technology (DST), Government of India under Grant TMD/CERI/BEE/2016/059(G).

ABSTRACT In this article, a new modulation scheme named Direct Current biased Optical Generalised Frequency Division Multiplexing (DCO-GFDM) for Visible Light Communications (VLC) is explored. The DCO-GFDM enhances spectral efficiency by slicing both grids on the time-frequency plane and uses a circularly rotating filter for pulse shaping. In the Circular Pulse shaped DCO-GFDM (CP-DCO-GFDM), Root Raised Cosine (RRC) pulse is widely employed. This destroys the orthogonality among sub-carriers and degrades the Bit Error Rate (BER) performance. Therefore, in this work, a Linearly Pulse shaped DCO-GFDM (LP-DCO-GFDM) is proposed to retain the orthogonality among the sub-carriers and simultaneously improve BER and Peak-to-Average Power Ratio (PAPR) performance. The performance of CP/LP-DCO-GFDM is studied under double sided clipping distortion that occurs at the Light Emitting Diode (LED). Presented simulation results agree well with the theoretical results. Additionally, we present an experimental validation of the LP-DCO-GFDM on a Universal Software Radio Peripherals (USRP) based VLC test bed. The experimental results, in terms of Error Vector Magnitudes (EVM)s, the received constellations, and the received spectrum in comparison with DCO-OFDM shows improved performance.

INDEX TERMS DC biased optical generalised frequency division multiplexing (DCO-GFDM), error vector magnitudes (EVM), linearly pulse shaped DCO-GFDM (LP-DCO-GFDM), universal software radio peripherals (USRP), visible light communications (VLC).

I. INTRODUCTION

EMERGING technologies, such as the Internet of Things (IoT), are causing exponential growth in data traffic [1]. In addition, other factors like the surge in online activities that include online gaming, e-business, huge social networking, and even the cheap data costs in some countries have resulted in increased data demands. Visible Light Communication (VLC) has been explored as a complementary technology to relieve the burden on the overcrowded Radio Frequency (RF) spectrum [2]. In addition to the benefits like huge unlicensed bandwidth, secure communication, and energy efficiency, VLC technology can enable services like Internet of Medical Things (IoMT) in healthcare environment where RF communication is undesirable [3]. Furthermore, Light Fidelity (Li-Fi) has been studied an enabler of vehicular communications. [6].

The ubiquitous presence of Light Emitting Diodes (LEDs) in the lighting infrastructure remains an impetus for VLC

technology. A light source can now be used for both illumination and wireless communication simultaneously. VLC uses Intensity Modulation (IM) to transmit data while Direct Detection (DD) is used at the receiver. In IM/DD, the data carrying signal must be real and unipolar to modulate the intensity of the optical source. Though single carrier modulations like On-Off Keying (OOK), Pulse Amplitude Modulation (PAM) and Pulse Position Modulation (PPM) can be easily implemented, problems like Inter Symbol Interference (ISI) critically affect their performance at higher data rates [4]. Consequently, several forms of multi-carrier modulations, such as Optical-Orthogonal Frequency Division Multiplexing (O-OFDM), have been explored for VLC in literature [5]. In these OFDM based modulation techniques, different symbols occupy different grids on the frequency plane and all occupy the same time grid. Furthermore, due to the inherent rectangular filtering in O-OFDM modulations, they give more Out-of-Band (OOB) emission that reduces power efficiency. In addition, the high Peak-to-Average Power Ratio (PAPR) gives more clipping distortion at the LED transmitter.

In order to address the foregoing challenges of O-OFDM systems, a DC biased Optical Generalised Frequency Division Multiplexing (DCO-GFDM) is introduced. With DCO-GFDM both the time and frequency grids are divided unlike in OFDM modulation where only the frequency grid is sliced [7]. For this reason, DCO-GFDM transmits multiple symbols on each sub-carrier and uses circularly rotating prototype pulse shaping filter on each time grid. In the context of the prototype filter, Root Raised Cosine (RRC) filter is widely employed in Circular Pulse shaped DCO-GFDM (CP-DCO-GFDM) and the performance is influenced by its roll-off-factor (α). However, the use of RRC makes the sub-carriers non-orthogonal leading to performance deterioration [8]. Therefore, in the present work, a Linearly pulse shaped DCO-GFDM (LP-DCO-GFDM) is introduced. This uses linear pulse shaping filters that offer an improved Bit Error Rate (BER) and PAPR performance by retaining the orthogonality of the sub-carriers. Moreover, the non-linear characteristics of front end LEDs will distort the transmitted signal and affect the performance. Thus, we study the effect of double sided clipping on the performance of CP/LP-DCO-GFDM and analytical expressions derived for its BER and PAPR under clipping distortion. The validity of the expressions is verified under different biasing conditions and practical LED power constraints. Finally, we use Universal Software defined Radio Peripheral (USRP) to experimentally validate the CP-DCO-GFDM and compare its performance to the conventional DCO-OFDM [9], [10].

The rest of the paper is organised as follows, Section II introduces the linear pulse shaping filters used in this work while Section III describes the proposed system model. Section IV presents the performance analysis of the system under clipping noise. Simulation results are given in Section V with experimental results presented in Section VI. Finally, Section VII concludes the paper.

II. PROLATE SEQUENCES

In [11], Slepian introduced a new set of band limited discrete orthogonal basis functions named Discrete Prolate Spheroidal Sequences (DPSS) or Slepian sequences. These are also termed as Multi-tapers. They generate an orthogonal basis within the analysis window, W, (in normalized units $0 < W < 0.5$) and are related to the time bandwidth product NW of the process under consideration, where, N is the number of observations of the corresponding process. In matrix form the generation of DPSS is represented by [11], [12]

$$\mathbf{G}(N, W)\mathbf{X}_l(N, W) = \lambda_l(N, W)\mathbf{X}_l(N, W), \tag{1}$$

in which

$$\mathbf{G}(N, W) = \begin{cases} \sin(2\pi W(m-n))/(\pi(m-n)), \\ \quad \text{for } m \neq n \text{ and } m, n = 0, 1, \ldots, N-1\,. \\ 2W, \qquad \text{for } m = n. \end{cases}$$

In (1), $\mathbf{X}_l(N, W)$ is the eigenvector matrix having eigenvectors $[x_n^{(l)}(N, W)]$ as samples from $n = 0, 1, \ldots, N-1$. Here, the eigenvectors $x_n^{(l)}(N, W)$ are called DPSS or Slepian sequences. Further, the eigenvalues $\lambda_l(N, W)$ measure the amount of energy concentrated in the band W. As per Slepian, only the first $L = 2NW$ multi-tapers, which all have $\lambda_l(N, W) \approx 1$, are needed to be considered as they possess the best possible energy concentration in the considered band, W. These multi-taper DPSS's are considered in the proposed LP-DCO-GFDM for the process of pulse shaping as described in the subsequent section.

III. SYSTEM MODEL

In this section, we describe the LP-DCO-GFDM system model, including the transmitter with a pre-clipping model (which is inevitable due to the limited dynamic range of the LED transmitter) and the receiver model. The complete system model considered in the present work is shown in Fig. 1 and the details of the proposed LP-DCO-GFDM transmitter is illustrated in Fig. 2. The main difference between DC biased Optical OFDM (DCO-OFDM) and DCO-GFDM is that the former transmits one symbol on each sub-carrier, whereas the latter transmits multiple symbols by relying on block based transmission. In addition, DCO-GFDM offers flexibility in the digital pulse shaping. This confines the signal well in time and frequency domain. Furthermore, DCO-GFDM prevents spectrum leakage with low OOB emission and uses a single cyclic prefix for multiple time slots to improve spectral efficiency. We consider a DCO-GFDM system with K sub-carriers with each sub-carrier having M sub-symbols in a block. Therefore, a block of $MK \times 1$ J-QAM complex symbols are taken in vector form as:

$$\mathbf{q} = \left[\mathbf{q}_0^\top \ \mathbf{q}_1^\top \ldots \mathbf{q}_{K-1}^\top\right]^\top, \tag{2}$$

which contains a $M \times 1$ vector on kth sub-carrier as $\mathbf{q}_k = [q_k(0)\ q_k(1) \ldots q_k(M-1)]^\top$. That is, $q_k(m)$ is a complex symbol on kth sub-carrier in the mth sub-symbol. Meanwhile, in order to obtain the real signal as per the requirement

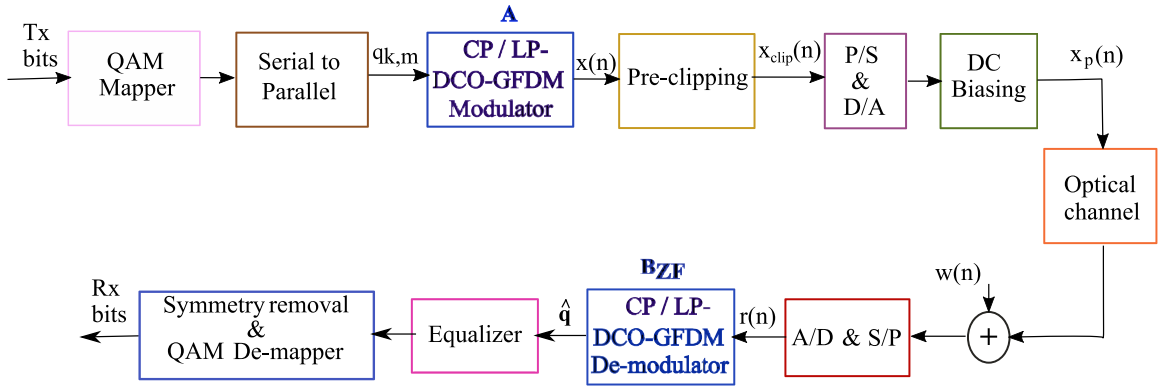

FIGURE 1. Illustration of the CP/LP-DCO-GFDM based IM/DD system.

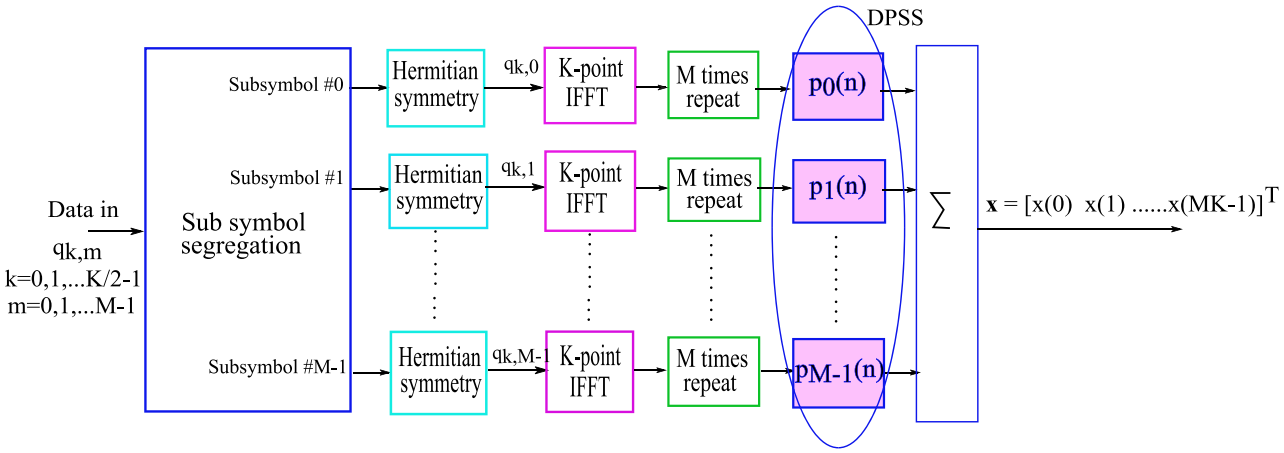

FIGURE 2. Details of LP-DCO-GFDM modulator.

of an IM/DD VLC system, the complex symbols in each sub-symbol should have Hermitian symmetry as:

$$\{q_k(m)\}_{k=0}^{K-1} = \left[q_0(m) \quad \{q_k(m)\}_{k=1}^{\frac{K}{2}-1} \quad q_{\frac{K}{2}}(m) \quad \{q_k(m)^*\}_{k=\frac{K}{2}-1}^{1}\right], \tag{3}$$

in which $q_0(m)$ and $q_{\frac{K}{2}}(m)$ are set to zero for all m. In DCO-GFDM, the data symbols in each sub-symbol are first oversampled and then passed through a pulse shaping filter followed by upconversion to the corresponding sub-carrier. Later, all the sub-symbols are summed up to produce DCO-GFDM signal as given by (4) [13], [14]

$$x(n) = \sum_{k=0}^{K-1}\sum_{m=0}^{M-1} q_k(m)p_{k,m}(n), \quad \text{for } n = 0, 1, \ldots MK-1 \tag{4}$$

where, $p_{k,m}(n)$ is the pulse shaping filter which is upconverted to kth sub-carrier for every k and is defined below for the two variants of DCO-GFDM considered in this work.

- *CP–DCO–GFDM:*

$$p_{k,m}(n) = p\left[(n-mK)_{modMK}\right].\exp\left(j2\pi\frac{k}{K}n\right). \tag{5}$$

- *LP–DCO–GFDM:*

$$p_{k,m}(n) = p_m(n).\exp\left(j2\pi\frac{k}{K}n\right). \tag{6}$$

In (5), $p(n)$ is a single circular rotating filter that rotates by K samples for every m. A Square Root Raised Cosine (SRRC) pulse with roll-off factor α is used in CP-DCO-GFDM as a pulse shaping filter. Alternatively, in this work we propose linear pulse shaping using $L = M$ multi-taper filters given by (6), with $p_m(n)$ being the mth multi-taper.

Representing all the samples in (4) in vector form results in $\mathbf{x}_g = [x(0), x(1), \ldots, x(MK-1)]^\top]$, and using the data vector $\mathbf{q}$ in (2), the time domain real DCO-GFDM signal vector in matrix form is given by [13]:

$$\mathbf{x_g} = \mathbf{Aq}, \tag{7}$$

where, the GFDM modulation matrix $\mathbf{A}$ (of size $MK \times MK$) is,

$$\mathbf{A} = \left[\mathbf{F} \quad \mathbf{T_1F} \quad \ldots \quad \mathbf{T_{K-1}F}\right], \tag{8}$$

in which $\mathbf{F}$ is a filter matrix of size $MK \times M$. In LP-DCO-GFDM, the M columns of $\mathbf{F}$ contain M different DPSS sequences of length MK that are orthogonal to

each other, whereas in CP-DCO-GFDM, every mth column of $\mathbf{F}$ is obtained by circularly rotating the samples of $p(n), n = 0, 1, \ldots, MK-1$, mK times. That is in CP-DCO-GFDM, the first column of $\mathbf{F}$ contains the MK samples from $p(n)$, and the remaining columns are produced by circularly rotating the first column. In contrast, all the M columns of $\mathbf{F}$ in LP-DCO-GFDM are the M different Slepian multi-taper sequences. It should be noted that $\mathbf{F}^\top\mathbf{F} = \mathbf{I}$ which confirms the orthogonality among the columns. Furthermore, the diagonal matrix $\mathbf{T_i} = \text{diag}\{[\mathbf{e_i}^\top \cdots \mathbf{e_i}^\top]^\top\}$ is a $MK \times MK$ matrix with M concatenated copies of the vector $\mathbf{e_i} = [1, e^{j2\pi\frac{i}{K}}, \ldots e^{j2\pi\frac{i}{K}(K-1)}]^\top$. The modulated time domain signal generated is then transmitted through the front end LED transmitter with limited dynamic range. This non-linear LED transmitter will distort the signal on both sides. Thus, to limit the clipping distortion and to effectively utilize the limited dynamic range, pre-clipping, as shown in Fig. 1, is introduced in the signal according to [15], [16],

$$x_{clip}(n) = \begin{cases} l_{top}, & \text{if } x(n) \geq l_{top} \\ x(n), & \text{if } l_{bot} < x(n) \leq l_{top} \\ l_{bot} & \text{if } x(n) \leq l_{bot}, \end{cases} \tag{9}$$

where, l_{top} and l_{bot} are the normalised top and bottom clipping levels respectively. The clipping levels are determined from the front end biasing parameters of LED such as the variance of an time domain signal, $\sigma^2_{x(n)}$ and biasing power, P_{bias} of the LED with a dynamic range (P_{min}, P_{max}). Further, the mean average power of the pre-clipped signal does not exceed P_{mean} in accordance with eye safety limits. Now, the clipping levels are determined as $l_{bot} = (P_{min} - P_{bias})/\sigma_{x(n)}$ and $l_{top} = (P_{max} - P_{bias})/\sigma_{x(n)}$ similar to optical OFDM systems in [15], [16]. The amount of clipping introduced is controlled by l_{bot} and l_{top} values. The signal clipping in the ideal case would assume the values $l_{bot} = -\infty$ and $l_{top} = +\infty$. After the pre-clipping, a bias P_{bias} is added to achieve unipolar signal transmission through the LEDs. Using Bussgang and Central limit theorems, the received signal can be modelled by an independent clipping noise vector $(\mathbf{w_{clip}})$ with a variance σ^2_{clip} and Additive White Gaussian Noise (AWGN) noise vector $(\mathbf{w})$ with variance σ^2_w as given below [17], [18].

$$\mathbf{r} = g_{opt}K_a\mathbf{x_g} + g_{opt}\mathbf{w_{clip}} + \mathbf{w}. \tag{10}$$

It can be observed that the received signal in (10) is modeled in terms of unclipped signal $\mathbf{x_g}$ with an attenuation factor K_a. The attenuation factor K_a can be calculated similarly to that of DCO-OFDM as in [15], [16]. In (10), the optical path gain coefficient g_{opt} is defined in terms of average irradiance of the photodiode as in [7]. Now, the estimated symbols at the receiver are obtained by employing Zero-Forcing (ZF) receiver in DCO-GFDM demodulator. That is,

$$\hat{\mathbf{q}} = \mathbf{B_{ZF}}\mathbf{r}, \tag{11}$$

in which $\mathbf{B_{ZF}} = (\mathbf{A}^H\mathbf{A})^{-1}\mathbf{A}^H$ is computed by using the modulation matrix $\mathbf{A}$ defined in (7). Alternatively, we can employ Minimum Mean Square Error (MMSE) receiver for a slightly better response. Finally, the transmitted bits are extracted by processing the estimated symbols $\hat{\mathbf{q}}$ as depicted in Fig. 1.

IV. PERFORMANCE ANALYSIS UNDER CLIPPING NOISE STATISTICS

A. BER PERFORMANCE ANALYSIS

The non-linear characteristics of the front end device introduce clipping on both sides of the signal and determine the electrical signal to Noise Ratio (SNR) $(\gamma_{b(ele)})$, which in turn affects the BER performance. The BER performance of CP/LP-DCO-GFDM for J-QAM, under the induced double sided clipping distortion, can be expressed analytically as [19], [20]

$$BER = 2\left(\frac{\sqrt{J}-1}{\sqrt{J}\log_2 J}\right)\text{erfc}\left(\sqrt{\frac{3\log_2 J}{2(J-1)}.(\Gamma_{b(eff)})}\right) + \left(\frac{\sqrt{J}-1}{\sqrt{J}\log_2 J}\right)^2\text{erfc}^2\left(\sqrt{\frac{3\log_2 J}{2(J-1)}.(\Gamma_{b(eff)})}\right), \tag{12}$$

where, $\Gamma_{b(eff)}$ is the electrical SNR of the clipped/distorted signal. In terms of the unclipped signal electrical SNR $\gamma_{b(ele)} = E_{b(ele)}/N_0$ it is given as:

$$\Gamma_{b(eff)} = \frac{K_a^2}{\xi\left(\frac{R_B\sigma^2_{c1ip}}{P_{b(e1ec)}} + \frac{R_B\gamma^{-1}_{b(elec)}}{G_{DC}}\right)}, \tag{13}$$

in which ξ is the Noise Enhancement Factor (NEF) whose values for the kth sub-carrier is obtained from:

$$\xi = \sum_{n=0}^{N-1}|[\mathbf{B_{ZF}}]_{k,n}|^2. \tag{14}$$

The value of ξ is equal for all sub-carriers and becomes unity in LP-DCO-GFDM due to the orthogonality between sub-carriers. The bandwidth utilisation factor $R_B = \frac{M(K-2)}{MK}$ and the factor that represents the attenuation of useful electrical power due to added bias is $G_{DC} = \frac{\sigma^2_{x(n)}}{\sigma^2_{x(n)}+P^2_{bias}}$ for both CP/LP-DCO-GFDM. In particular, the attenuation factor K_a and the clipping noise power σ^2_{clip} in CP/LP-DCO-GFDM are similar to DCO-OFDM and is given as [15],

$$K_a = Q(l_{bot}) - Q\big(l_{top}\big), \tag{15}$$

and,

$$\sigma^2_{clip} = \sigma^2_{x(n)}\left(1 - K_a^2\right) - \triangle\sigma^2, \tag{16}$$

where,

$$\triangle\sigma^2 = \sigma^2_{x(n)}\Big(1 - \Big[Q(l_{bot}) - Q\big(l_{top}\big) + \phi(l_{bot})l_{bot} - \phi\big(l_{top}\big)l_{top} + (1 - 2Q(l_{bot}))l^2_{bot} + Q\big(l_{top}\big)l^2_{top}\Big]$$

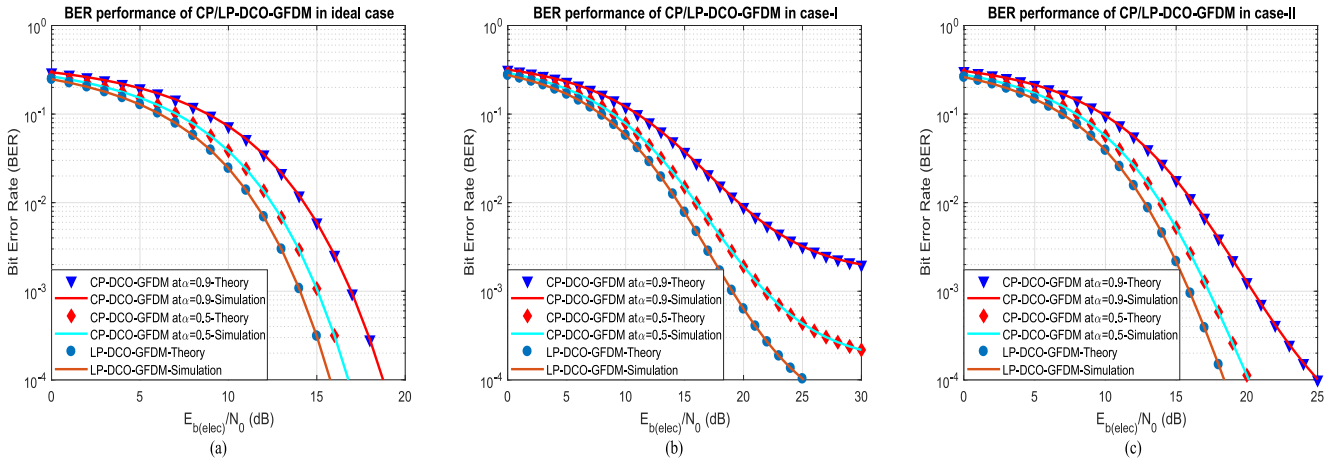

FIGURE 3. Comparison of BER performance of CP/LP-DCO-GFDM system for 4-QAM under AWGN channel.

$$+\left[\phi(l_{bot})-\phi\left(l_{top}\right)+(1-Q(l_{bot}))l_{bot}+Q\left(l_{top}\right)l_{top}\right]^2\Big). \tag{17}$$

Here, $Q(.)$ is the complementary cumulative distribution function (CCDF) given by:

$$Q(v)=\frac{1}{\sqrt{2\pi}}\int_v^{\infty}\exp\left(-\frac{z^2}{2}\right)dz. \tag{18}$$

B. PAPR ANALYSIS

The PAPR of the clipped time domain signal is defined as,

$$PAPR=\frac{max\left(\left|x_{clip}^2\right|\right)}{E\left[x_{clip}^2\right]}. \tag{19}$$

The PAPR CCDF for the clipped CP/LP-DCO-GFDM signal can be obtained using the approach in [21] for the clipping levels l_{bot} and l_{top} as below.

$$F_{PAM}(x)=\begin{cases}1-\left[2\left(1-Q\left(\sqrt{g\left(l_{bot},l_{top}\right)x}\right)\right)-1\right]^{MK}; & \text{if } 0\le x<\theta_{min}\\ 1-\left[1-Q\left(\sqrt{g\left(l_{bot},l_{top}\right)x}\right)\right]^{MK}; & \text{if } \theta_{min}\le x<\theta_{max}\\ 0; & \text{if } x\ge\theta_{max}\end{cases} \tag{20}$$

where,

$$\theta_{min}=\frac{l_{bot}^2}{g\left(l_{bot},l_{top}\right)},\quad\text{and}\quad\theta_{max}=\frac{l_{top}^2}{g\left(l_{bot},l_{top}\right)}. \tag{21}$$

Here $g(l_{bot},l_{top})$ is a function that defines the average power of the signal and is given as [15], [16]:

$$g\left(l_{bot},l_{top}\right)=\left(l_{top}^2-1\right)Q\left(l_{top}\right)-\left(l_{bot}^2-1\right)Q(l_{bot})+l_{bot}^2+l_{bot}\phi(l_{bot})-l_{top}\phi\left(l_{top}\right). \tag{22}$$

C. SPECTRAL ANALYSIS

The theoretical analysis of the Power Spectral Density (PSD) of CP/LP-DCO-GFDM is useful in the computation of OOB emission power and can be computed by using [22].

$$S_{x_g}(f)=\lim_{T\to\infty}\left(\frac{1}{T}\mathbb{E}\left[\left|F\left(x_g(t)\right)\right|^2\right]\right), \tag{23}$$

where, $F(.)$ represents the Fourier Transform and T is duration of one CP/LP-DCO-GFDM symbol. The concatenation of multiple symbols $x_g(t)$ is represented by:

$$x_g(t)=\sum_{v=-\infty}^{\infty}\sum_{m=0}^{M-1}\sum_{k=0}^{K-1}q_k(m)p_m(t-vMT_s)e^{-j2\pi\frac{k}{T_s}t}+P_{bias}, \tag{24}$$

in which T_s is the duration of each sub-symbol, P_{bias} is the DC-bias added to make the signal unipolar, and $p_m(t)$ is the continuous prototype filter. The final expression for PSD can be obtained as [7]:

$$S_{x_g}(f)=\frac{\sigma_d^2}{MT_s}\left[\sum_{m,k}\left|P_m\left(f-\frac{k}{T_s}\right)\right|^2+\sum_{m,k}\left|P_m\left(f-\frac{K-k}{T_s}\right)\right|^2\right]+\frac{P_{bias}^2}{MT_s}\delta(f), \tag{25}$$

where $\delta(.)$ represents impulse function and σ_d^2 represents the variance of the data symbols. It can be observed that the PSD is symmetrical and has a DC value at zero frequency.

V. SIMULATION RESULTS

The BER performance of the proposed LP-DCO-GFDM system is investigated under double sided clipping distortion and compared with CP-DCO-GFDM system using SRRC pulse with a roll-off factor α. For the BER investigation, three different clipping cases as considered; similar

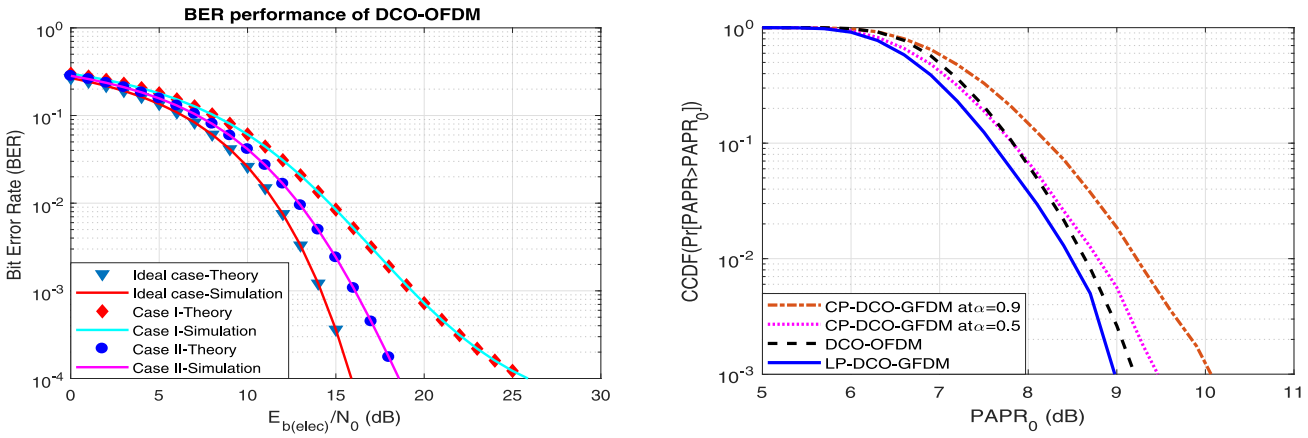

FIGURE 4. (a) BER performance of DCO-OFDM system for 4-QAM under AWGN channel and (b) PAPR performance of CP/LP-DCO-GFDM and DCO-OFDM under ideal clipping scenario.

TABLE 1. Simulation cases [15], [16].

Parameter	Ideal Case	Case-I	Case-II
Average optical power (P_{mean})	10 mW	10 mW	15 mW
Biasing power (P_{bias})	P_{mean}	9.8 mW	14.8 mW
Variance σ_x	$P_{mean}/2$	4.9 mW	7.4 mW
Lower clipping level (l_{bot})	-2	-0.98	-1.32
Upper clipping level (l_{top})	∞	8.2	4.76

to the optical OFDM system report in [15], [16] for Vishay TSHG8200 LED. The three different cases for different average optical power P_{mean} and biasing power P_{bias} with their corresponding clipping levels are presented in Table 1. The robustness of the BER expression which is a function of modified eSNR ($\Gamma_{b(eff)}$) is verified through unclipped signal electrical SNR ($\gamma_{b(elec)}$) using Monte-Carlo simulations in MATLAB. We consider 256 sub-carriers (K) each with 5 sub-symbols (M) and 4-QAM constellation. The BER performance of DCO-OFDM under double sided clipping is also simulated under similar conditions for comparison purpose [15].

The BER performance of DCO-GFDM system under three cases considered is shown in Fig. 3 (a). The plots show a close match between theoretical and simulation results in all the cases. In Fig. 3 (a) with ideal case where $l_{bot} = -2$ and $l_{top} = \infty$, the clipping noise is low. For Case-I with an average optical power $P_{mean} = 10$ mW and a lower biasing power P_{bias} compared to case-II, the amount of clipping is more. This results in deteriorated error performance in all the cases under investigation as depicted in Fig. 3 (b). As the biasing power, P_{bias}, is increased to the middle of the dynamic range with more P_{mean} as in Case-II, the improvement in performance can be noticed in Fig. 3 (c). Therefore, for a DCO-GFDM system, a front end device with more P_{mean} can be selected just like DCO-OFDM as mentioned in [15]. Furthermore, in each case, the CP-DCO-GFDM with SRRC pulse with a roll-off factor α under performing compared to the proposed LP-DCO-GFDM system with DPSS as a prototype filter. This is due to the reduction in NEF (ξ) given in (14), which is obtained due to the orthogonality between sub-carriers. The value of this ξ is higher in the CP-DCO-GFDM using SRRC pulse where the sub-carriers are non-orthogonal. This non-orthogonality between sub-carriers gives rise to successive interference which increases with roll-off factor α and degrades the performance as shown in Fig. 3. It can also be noticed that the performance of LP-DCO-GFDM matches that of DCO-OFDM as presented in Fig. 4 (a), but with improved spectral efficiency due to the multiple symbols per sub-carrier.

Moreover, the PAPR of LP-DCO-GFDM is compared with CP-DCO-GFDM and DCO-OFDM and depicted in Fig. 4 (b) under conditions given in Table 1. It can be noticed that the LP-DCO-GFDM outperforms CP-DCO-GFDM for both values of roll-off factor α. PAPR gains of 1 dB and 0.5 dB in LP-DCO-GFDM are observed compared to CP-DCO-GFDM for values of $\alpha = 0.9$ and $\alpha = 0.5$, respectively. With respect to DCO-OFDM, a nominal increase of 0.2 dB is observed. The improvement in performance pertains to the orthogonal nature of the sub-carriers in LP-DCO-GFDM and multi-taper filters. Similar trends are noticed in the other clipping scenario cases which are not shown due to space constraints.

VI. EXPERIMENTAL RESULTS

In this section, the experimental procedure for the validation of LP-DCO-GFDM and the corresponding results are presented. The details of different processing steps involved in the experimental demonstration along with hardware are illustrated in Fig. 5. The baseband modulation along with essential processing steps like up-sampling and pulse shaping are accomplished in Lab-view PC. Later, the frequency conversion from low to high and vice versa is performed by using USRP boards for which Ettus x300 and N210 are utilized at transmitter and receiver, respectively. The signal from the transmitter USRP is made unipolar by adding a suitable DC bias at the Bias Tee and then given to LED

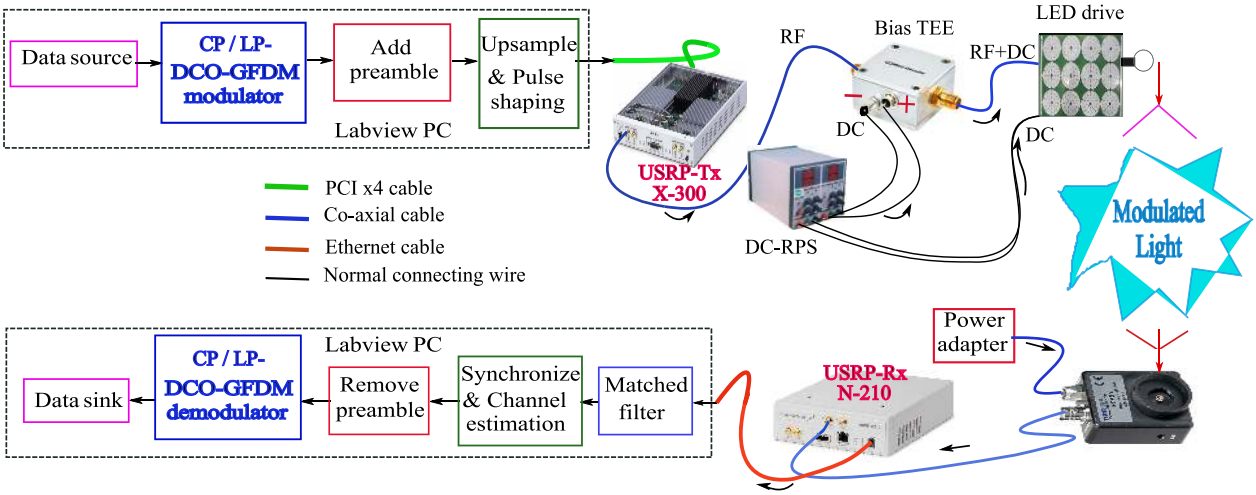

FIGURE 5. An illustration of the experimental set-up for the CP/LP-DCO-GFDM implementation.

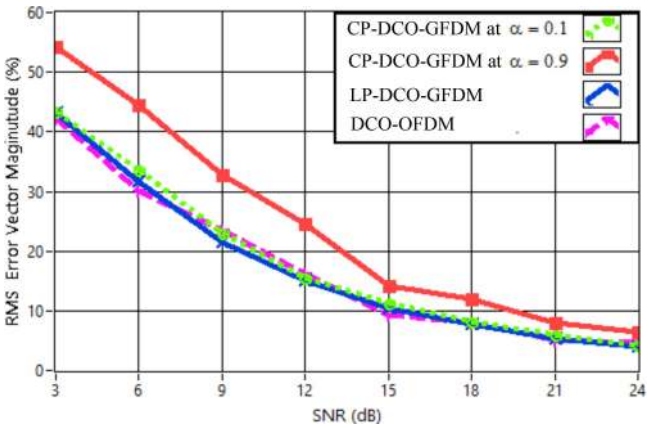

FIGURE 6. EVM comparison of CP/LP-DCO-GFDM for 4-QAM.

circuitry to modulate the light intensity. Subsequently, the modulated light propagated through the free space is received by a photodiode at the receiver. The electrical signal produced is then down converted by the receive USRP board. The receiver USRP sends the down converted data packet to Lab-view PC where the necessary processes like the matched filtering, synchronization, and equalization are accomplished to demodulate the data packet and finally retrieve the transmitted information as depicted in Fig. 5. The experimental demonstration of the CP/LP-DCO-GFDM is verified primarily by the metrics Root Mean Square (RMS) Error Vector Magnitude (EVM), received magnitude spectrums, and received constellations. The RMS-EVM parameter is calculated by using,

$$EVM(\%) = \sqrt{\frac{\frac{1}{N}\sum_{n=0}^{N-1}\left[\left(A_n - \hat{A}_n\right)^2 + \left(B_n - \hat{B}_n\right)^2\right]}{\frac{1}{N}\sum_{n=0}^{N-1}\left[A_n^2 + B_n^2\right]}} \times 100. \quad (26)$$

TABLE 2. Experimental set-up parameters.

Name of the parameter	Value
Number of sub carriers (K)	64
Number of Sub-symbols (M)	5
Number of DCO-GFDM symbols in each packet	4
Null carriers	16
Cyclic prefix	8
Preamble and zero pad length	128
Pulse shaping (RRC) length	8
Oversampling factor (L) and IQ sampling rate (MHz)	4
Modulation order (J)	4, 16-QAM

where, A_n and B_n are the in-phase and quadrature phase values of ideal symbols, $\hat{A}_n$ and $\hat{B}_n$ are the in-phase and quadrature phase values of receiving symbols, respectively.

The experimental parameters are listed in Table 2. In the implementation of CP/LP-DCO-GFDM, the number of sub-carriers $K = 64$ and sub-symbols $M = 5$ are considered. Along with CP-DCO-GFDM using SRRC pulse with roll-off factor α, DCO-OFDM with the same number of sub-carriers are also examined in the comparative analysis. 4-QAM and 16-QAM constellations are assumed in the implementation of the system and accordingly, the RMS-EVM comparison of LP-DCO-GFDM with the corresponding modulation is depicted in Fig. 6 for 4-QAM constellation. It is observed that CP-DCO-GFDM for $\alpha = 0.9$ is giving higher EVM values among all the cases which are due to the more self interference that occurs because of the high roll-off portion. As the value of α is decreased to 0.1, the reduction in RMS-EVM can be noticed which is due to the decrease in NEF (ξ) that occurs because of the reduction in self interference. In contrast, the proposed LP-DCO-GFDM is giving low RMS-EVM values of around $2-3.5\%$ less than the CP-DCO-GFDM with $\alpha = 0.1$ particularly at low SNRs in the range $5-10$ dB. This is achieved by improving the orthogonality among the sub-carriers. Meanwhile, it should be noted that the EVM performance of LP-DCO-GFDM reaches that of DCO-OFDM, but with improved spectral

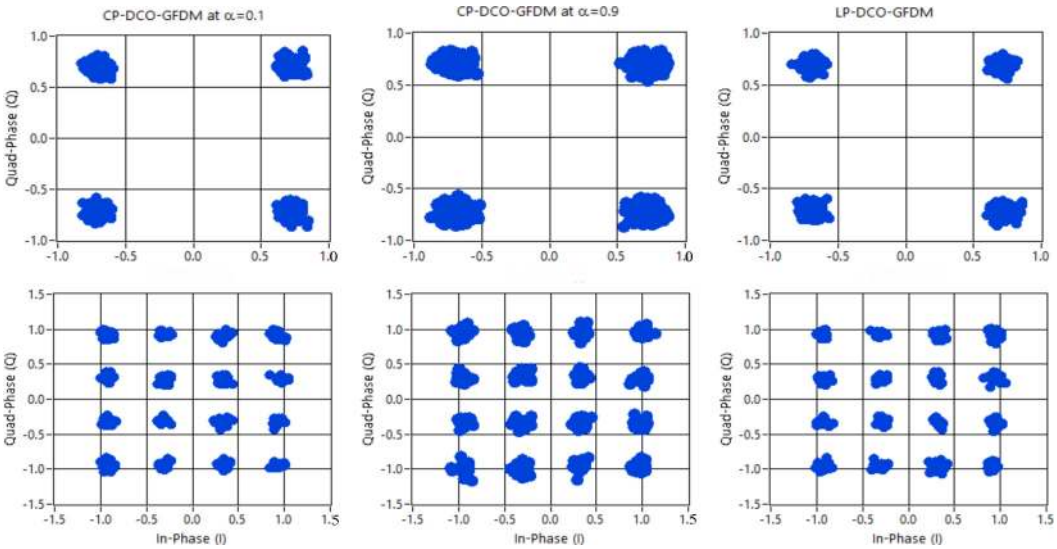

FIGURE 7. Received constellations for 4-QAM (above) and 16 QAM (below) in different cases of LP-DCO-GFDM at a sampling rate of 4 M samples/sec and an SNR = 20 dB.

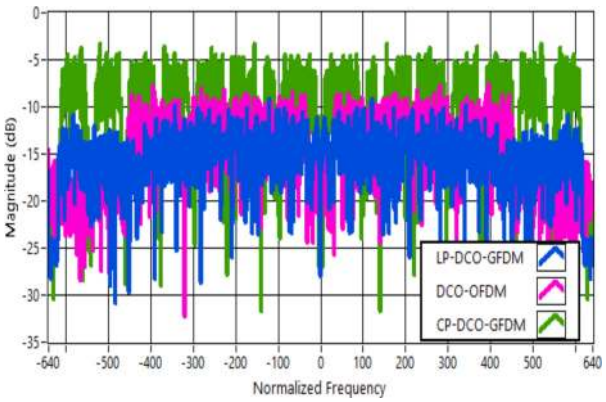

FIGURE 8. Comparison of received spectrums.

efficiency, which we get by sending multiple symbols on each sub-carrier. The EVM performance can be effectively indicated by the shape of the received constellations at an SNR of 20 dB as shown in Fig. 7 for 4-QAM and 16-QAM. The amplitude variations in the received symbols can be noted under different cases. For 16-QAM, a similar trend in EVM performance is observed, but at $2-3\%$ higher than 4-QAM and is not shown due to space constraints.

The received magnitude spectrums for the modulations under consideration in real time are compared in Fig. 8 where the frame length is made equal in all and 25% of the sub-carriers are set to nulls. Furthermore, the CP-DCO-GFDM spectrum is plotted for the case of $\alpha = 0.1$. It can be verified that the spectrums are symmetrical with respect to the middle sub-carrier as given analytically in (25) which is valid for DCO-OFDM and also for when $M = 1$ with a rectangular pulse. Mainly, the OOB emission of LP-DCO-GFDM is -14.2 dB which is 5 dB more than that of CP-DCO-GFDM. This is due to the deep side lobes of SRRC used in the latter. Nevertheless, the OOB emission in LP-DCO-GFDM is 4 dB less compared to that of DCO-OFDM which shows

TABLE 3. Experimentally achieved results in different cases.

System type	BER		Estimated SNR	OOB
	SNR = 5 dB	SNR = 20 dB	dB	[dB]
CP-DCO-GFDM at $\alpha = 0.9$	0.3581	1.131×10^{-3}	21.21	-14.8
CP-DCO-GFDM at $\alpha = 0.1$	0.2439	3.219×10^{-4}	23.39	-19.2
LP-DCO-GFDM	0.2337	2.216×10^{-4}	23.86	-14.2
DCO-OFDM	0.2419	2.813×10^{-4}	24.79	-10

considerable power efficiency. The experimental OOB, BER and esiamted SNR at the receiver are given in Table 3. The estimated SNR values at the receiver are computed from the Mean Square Error (MSE) in the computation of channel estimate. A lower MSE results in better SNR estimates at the receiver which signifies better detection accuracy. It can be noticed that LP-DCO-GFDM achieves lower BER and better estimated SNR than CP-DCO-GFDM and on a par with DCO-OFDM.

VII. CONCLUSION

In this article, we have introduced LP-DCO-GFDM that used linear pulse shaping to retain the orthogonality among the sub-carriers, unlike the traditional CP-DCO-GFDM in which circular pulse shaping is used. The performance of the LP-DCO-GFDM under the inevitable double sided clipping has been investigated for the VLC systems and the analytical expressions for BER and PAPR are derived. Simulation results showed a close match with the theoretical results and improved performance over CP-DCO-GFDM under different clipping scenarios. Further, the proposed modulation technique has been experimentally demonstrated in a real time VLC testbed. The experimentally attained results for RMS-EVM, received constellation and the magnitude spectrum have showed that LP-DCO-GFDM performance is similar to DCO-OFDM, but with a low OOB emission and improved spectral efficiency.

REFERENCES

[1] L. I. Albraheem *et al.*, "Toward designing a Li-Fi based hierarchical IOT architecture," *IEEE Access*, vol. 6, pp. 40811–40825, 2018.

[2] S. Zvanovec *et al.*, "Visible light communications towards 5G," *Radioengineering*, vol. 24, no. 1, pp. 1–8, Apr. 2015.

[3] M. Ayyash *et al.*, "Coexistence of Wi-Fi and Li-Fi toward 5G: Concepts, opportunities, and challenges," *IEEE Commun. Mag.*, vol. 54, no. 2, pp. 64–71, Feb. 2016.

[4] J. M. Kahn and J. R. Barry, "Wireless infrared communications," *Proc. IEEE*, vol. 85, no. 2, pp. 265–298, Jun. 1997.

[5] D. Karunatilaka, F. Zafar, V. Kalavally, and R. Parthiban, "LED based indoor visible light communications: State of the art," *IEEE Commun. Surveys Tuts.*, vol. 17, no. 3, pp. 1649–1678, 3rd Quart., 2015.

[6] M. Katz and I. Ahmed, "Opportunities and challenges for visible light communications in 6G," in *Proc. 2nd 6G Wireless Summit (6G SUMMIT)*, 2020, pp. 1–5.

[7] V. Kishore and V. Mani, "A DC biased optical generalised frequency division multiplexing for IM/DD systems," *Phys. Commun.*, vol. 33, pp. 115–122, Apr. 2020.

[8] V. Kishore and V. Mani, "An LED modelled GFDM for optical wireless communications," *Int. J. Electron. Commun.*, vol. 101, pp. 54–61, Feb. 2019.

[9] S. P. Valluri and V. Mani, "Investigation of blind CFO estimation for GFDM system using universal software radio peripheral: Theory, simulations and experiments," *IET Commun.*, vol. 13, no. 8, pp. 1936–1944, Aug. 2019.

[10] K. Vejandla *et al.*, "A tunable energy signal for intensity modulation and direct detection systems: Theory, simulations, and experiments," *IEEE Photon. J.*, vol. 12, no. 1, pp. 1–12, Feb. 2020.

[11] D. Slepian, "Prolate spheroidal wave functions, Fourier analysis, and uncertainty: The discrete case," *Bell Syst. Tech. J.*, vol. 57, no. 5, pp. 1371–1430, 1978.

[12] S. K. Bandari, V. V. Mani, and A. Drosopoulos, "Multi-taper implementation of GFDM," in *Proc. IEEE Wireless Commun. Netw. Conf.*, 2016, pp. 1–5.

[13] A. Farhang, N. Marchetti, and L. E. Doyle, "Low-complexity modem design for GFDM," *IEEE Trans. Signal Process.*, vol. 64, no. 6, pp. 1507–1518, Nov. 2016.

[14] A. RezazadehReyhani, A. Farhang, and B. Farhang-Boroujeny, "Circularly pulse-shaped waveforms for 5G: Options and comparisons," in *Proc. IEEE Global Commun. Conf. (GLOBECOM)*, 2015, pp. 1–7.

[15] S. Dimitrov, S. Sinanović, and H. Haas, "Clipping noise in OFDM based optical wireless communication systems," *IEEE Trans. Commun.*, vol. 60, no. 4, pp. 1072–1081, Apr. 2012.

[16] K. Vejandla, S. Kollikonda, and V. M. Vakamulla, "Performance analysis of PAM-DMT under double sided signal clipping in IM/DD based systems," in *Proc. Nat. Conf. Commun. (NCC)*, 2020, pp. 1–6.

[17] J. A. Rice, *Mathematical Statistics and Data Analysis*, 2nd ed. London, U.K.: Duxbury, 1995.

[18] J. J. Bussgang, "Crosscorrelation functions of amplitude-distorted Gaussian signals," Res. Lab. Electron., Massachusetts Inst. Technol. Cambridge, MA, USA, Rep. 216, Mar. 1952.

[19] N. Michailow *et al.*, "Generalized frequency division multiplexing for 5th generation cellular networks," *IEEE Trans. Commun.*, vol. 62, no. 9, pp. 3045–3061, Aug. 2014.

[20] S. K. Bandari, A. Drosopoulos, and V. V. Mani, "Exact SER expressions of GFDM in Nakagami-*m* and Rician fading channels," in *Proc. Eur. Wireless 21th Conf.*, 2015, pp. 1–6.

[21] J. Wang, Y. Xu, X. Ling, R. Zhang, Z. Ding, and C. Zhao, "PAPR analysis for OFDM visible light communication," *Opt. Exp.*, vol. 24, no. 24, pp. 27457–27474, Nov 2016.

[22] T. van Waterschoot, V. L. Nir, J. Duplicy, and M. Moonen, "Analytical expressions for the power spectral density of CP-OFDM and ZP-OFDM signals," *IEEE Signal Process. Lett.*, vol. 17, no. 4, pp. 371–374, Apr. 2010.